European Journal of Mechanics / B Fluids 89 (2021) 64–71

Contents lists available at ScienceDirect

European Journal of Mechanics / B Fluids

journal homepage: www.elsevier.com/locate/ejmflu

Diurnal continental shelf waves with a permeable coastal boundary: Application to the shelf northwest of Norway

Jan Erik H. Weber [a,*], Eli Børve [a,b]

[a] Department of Geosciences, University of Oslo, Norway
[b] Akvaplan-Niva AS, Fram Centre, Tromsø, Norway

ARTICLE INFO

Article history:
Received 25 March 2021
Accepted 7 May 2021
Available online 11 May 2021

Keywords:
Diurnal waves
Lagrangian drift
Permeable boundary
Robin condition

ABSTRACT

Spatially damped continental shelf waves (CSWs) with diurnal tidal frequency outside Lofoten–Vesterålen in north-west Norway are studied theoretically for an idealized shelf topography. Wave damping is caused by the exchange of fluid on the shelf with an inner archipelago through a permeable coastline. This exchange is modelled by the application of a Robin condition at the coastal boundary. It is shown that CSWs with diurnal frequencies are possible in a small wave number range centred around zero group velocity. By calculating the nonlinear radiation stress components in the spatially damped CSWs, we find the time- and depth averaged Lagrangian mean drift current to second order along the coast. We show that the Lagrangian mean drift current is independent of the value of the damping coefficient, however small, as long as it is nonzero. This illustrates the singular behaviour of the Lagrangian wave drift problem for CSWs.

1. Introduction

We study sub-inertial wave motion over variable bottom topography. Longuet-Higgins [1,2] has described how such waves can propagate along a sloping bottom. The focus here is on wave motion along a continental shelf that is limited laterally by a coastal boundary; see e.g. Buchwald and Adams [3]. Such waves have become known as continental shelf waves (CSWs). The classic investigation on how CSWs are generated by the wind is that of Gill and Schumann [4]. We here focus on the shelf west of Norway. Traditionally, wind systems hitting the southwestern part of Norway has a storm track with an oblique angle to the coast. This generates CSWs that propagate northward along the Norwegian continental shelf, see e.g. [5] and [6]. These generation events are more frequent (and stronger) in the autumn and the winter, but they are in all cases sporadic.

A more regular mechanism for the generation of CSWs is the tidal diurnal motion, in particular, strong tidal motion through straits. We here refer to [7–9] for the generation of CSWs along the Australian shelf from tides in the Bass Strait. Even in cases without a strait, CSWs with diurnal tidal frequency may be generated on the shelf slope if the local group velocity is close to zero due to changes in topography; see [10] for the shelf near St. Kilda in the UK, and [11] for the Greenland shelf.

In north Norway, the tidally driven Moskstraumen is a clear parallel to the tidal motion in the Australian Bass strait, pressing water back and forth across the depth contours of the shelf outside Lofoten. The cross-shelf transport has been modelled in [12]. For the interested reader, Moskstraumen is the famously strong Lofoten Maelstrom with written accounts back to mediaeval times; see Gjevik et al. [13]. In Fig. 1 we have inserted a map of the Norwegian coastal area, with special reference to the Lofoten–Vesterålen region.

Usually, in modelling CSWs, the coastline is taken to be a solid wall. However, along the Norwegian coast there are a myriad of small islands and narrow fjords with a lateral scale much smaller than the CSW wavelength, as is evident from Fig. 1. Hence, since CSWs have a velocity component normal to the depth contours, which usually follows the coastline, there will be an exchange of fluid between the shelf and the narrow fjords and small islands. In the fjord system, the dissipation will be considerable. This will remove energy from the CSW, and lead to spatial damping as the wave propagates along the shelf slope. We note that this phenomenon is a clear parallel to the damping of surface waves over a permeable seabed by Reid and Kajiura [14]; see also [15] for surface waves over coral reefs.

We demonstrate that a non-zero velocity normal to the coastline inevitably will lead to a spatial damping of the CSWs. This is done by applying a Robin condition [16,17] at the coastal boundary. The Robin condition is a weighted combination of Dirichlet boundary conditions and Neumann boundary conditions and is common in many branches of physics. The Robin condition, through a small parameter, allows for a small velocity normal to the coastline, which is exactly what happens when we have

* Corresponding author.
E-mail address: j.e.weber@geo.uio.no (J.E. Weber).

https://doi.org/10.1016/j.euromechflu.2021.05.003

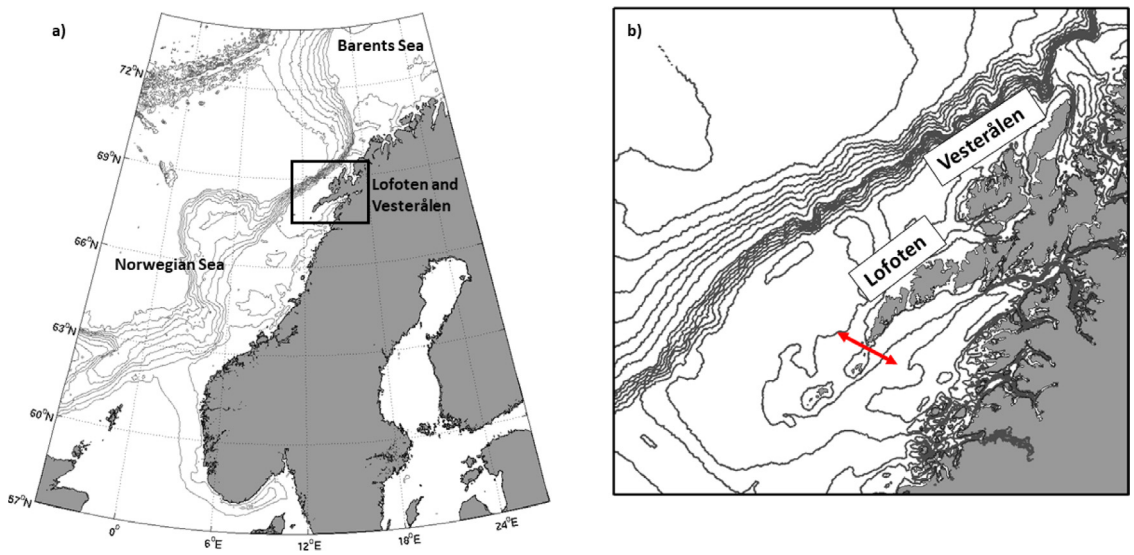

Fig. 1. (a) Map of the Norwegian coastal area with bottom contours. The relevant region here is the narrow shelf outside Lofoten and Vesterålen. (b) Close-up of the Lofoten–Vesterålen region where a red arrow indicates the position of Moskstraumen.

an inner archipelago with narrow fjords and small islands. The damping rate is then obtained as a function of the small Robin parameter.

As pointed out by Phillips [18], the vertically integrated flow between material surfaces (bottom and free surface) yields the Lagrangian volume fluxes. These fluxes are forced by the radiation stresses; see [19]. Weber and Drivdal [20] calculate the Lagrangian mean drift when the wave decay is due to bottom friction, which also affects the mean flow. Similar calculations are made in the present paper, where the wave decay is due to the nonzero flux condition at the permeable coastal boundary. Now the sloping shelf region is taken to be inviscid. This simplifies the calculation of the Lagrangian mean drift current, which is discussed for parameters that are typical for the shelf outside Lofoten.

2. Linear analysis for idealized bottom profiles and an impermeable coastal wall

We first discuss the presences of CSWs with diurnal frequency outside Lofoten–Vesterålen with the usual adoption of a solid coastal wall. In a forthcoming paper [21], it is found from a barotropic numerical model for tidal motion that a distinct amplification of the current speed occurs in the Lofoten–Vesterålen region for the diurnal K_1 tidal component. This is shown in Fig. 2, where the intensity of the red colour marks the areas with prominent K_1 tidal current amplification. The amplification of the K_1 tidal current through Moskstraumen is closely related to the distortion of the northward propagating tidal wave when it interacts with the Lofoten archipelago. The tidal wave is scattered and deflected around the island chain resulting in an east–west pressure gradient in the southern Lofoten, which enhances the tidal flow through Moskstraumen. The tidal flow is forced across the shallow ridge extending southwestward from the archipelago, which further enhances the current speed amplitude. Outside Vesterålen, on the other hand, the amplification in the K_1 tidal current amplitude cannot be explained by topographic features along the narrow and shallow shelf. Here, the K_1 amplification has been attributed to generation/conversion to continental shelf waves with diurnal frequency [22,23].

The places of particular interest here are the steep shelf regions outside Vesterålen; see Fig. 1b. For a closer study, we have chosen three particular transects, depicted in Fig. 3.

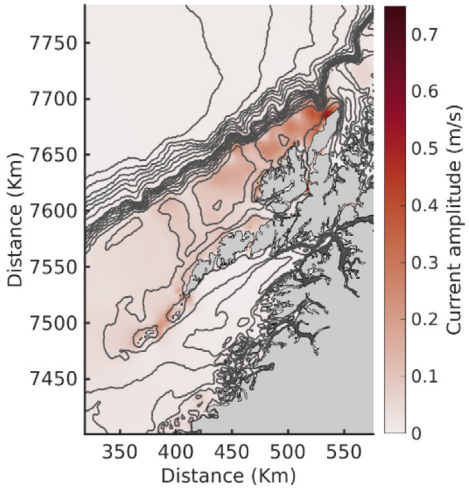

Fig. 2. Current speed amplification for the diurnal K_1 tidal component near Moskstraumen and along the shelf outside Vesterålen, based on Fig. 2 in [21].

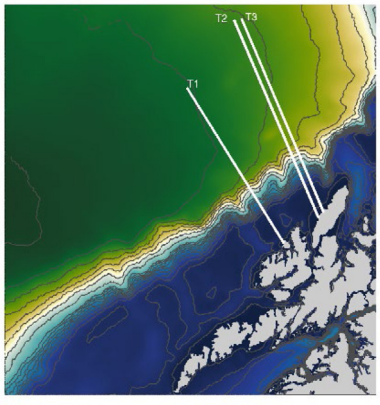

Fig. 3. Positions of transects T1, T2, T3 across the shelf outside Vesterålen.

We idealize the shelf geometry as in [3], but allow for a small flat inner shelf of width D and depth H_0, before the depth

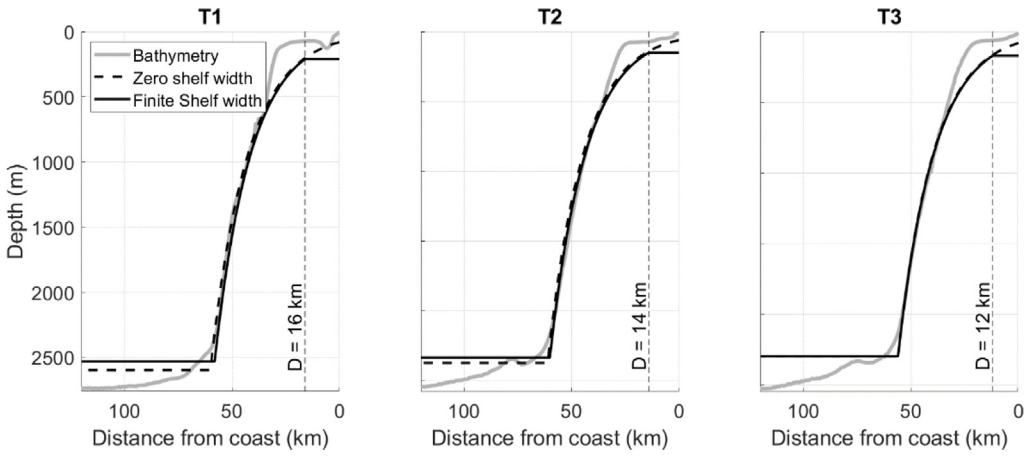

Fig. 4. Bottom profiles in transects T1, T2, T3 in Fig. 3.

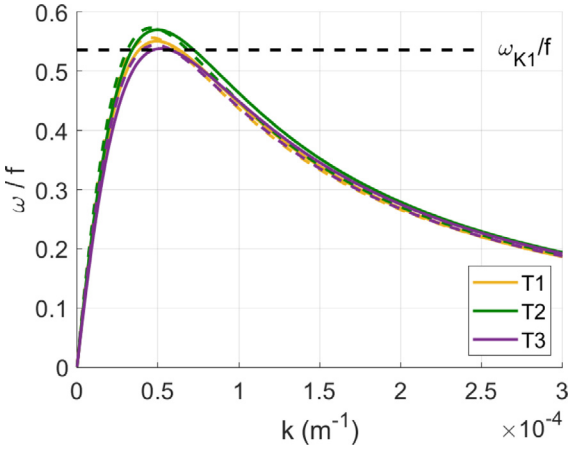

Fig. 5. Dispersion diagrams for transects T1, T2, T3 outside Vesterålen (first mode), showing non-dimensional frequency ω/f *vs* wave number k. Here f is the constant Coriolis parameter. Solid lines represent an inner shelf where $D \neq 0$, and dashed lines the case when $D = 0$. The upper horizontal dashed line is the non-dimensional tidal frequency for the K_1 component.

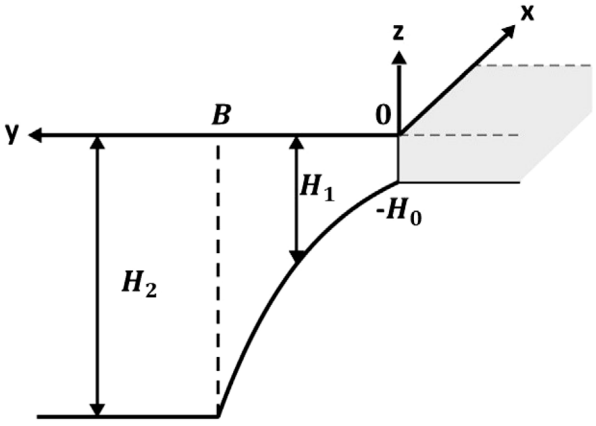

Fig. 6. A diagram showing the configuration with an exponential shelf, continued by a flat deep ocean. The shelf edge is located at $y = B$. The coastline at $y = 0$ is permeable (indicated by grey shading) and modelled by a Robin condition.

increases exponentially towards the deep ocean; see [6] and [11]. We place the x axis along the coast. The y axis is directed towards the sea, and the z axis is vertically upwards. The bottom profile is given by

$$H = \begin{cases} H_0, & -D \le y \le 0 \\ H_1 = H_0 \exp(2by), & 0 \le y \le B \\ H_2 = H_0 \exp(2bB), & y \ge B. \end{cases} \quad (1)$$

Here b is a constant describing the steepness of the slope, and B is the width of the sloping shelf.

Outside Vesterålen the flat part of the shelf is narrow, and we present the bottom profiles in Fig. 4 from transects T1, T2, T3 with a small D (solid black lines), and with $D = 0$ (dashed lines).

We use the analysis in [6] to compute the dispersion diagrams for the idealized exponential bottom profiles in Fig. 4. The results are depicted in Fig. 5.

We note from Fig. 5 that the effect on frequency of a narrow inner shelf is practically negligible in the region outside Vesterålen. More importantly, CSWs with a frequency corresponding to the diurnal K_1 component of the tidal motion are possible, as seen from the intersections with the upper broken line in Fig. 5. Furthermore, we note that at all transects the group velocity is close to zero for the diurnal frequency, which is similar to the findings in [11] for the Greenland shelf. This means that wave energy accumulates in the region, which may explain the current amplification along the shelf in Fig. 2. The existence of short CSWs on the shelf outside Vesterålen with diurnal frequency has also been reported by Moe et al. [22].

3. Linear waves with a robin condition at the coast

Having established that CSWs with a diurnal frequency may form in the Lofoten–Vesterålen region, we proceed to investigate some non-linear properties of these waves. For a solid coastal wall at $y = 0$, this problem has been studied in [20]. However, it is fair to say that the western coast of Norway bordering the continental shelf is far from impermeable. We note from Fig. 1 that this region contains a myriad of narrow fjords and small islands through which the shelf water may intrude. Therefore, we adapt a novel approach, and take that the coastal boundary is partly permeable. This has important consequences for the wave-induced drift, as will be shown in the following sections.

The linear wave problem starts out in a classic fashion [3,4]. We have already shown that the effect of a narrow, flat inner shelf outside Lofoten can be neglected. Our idealized shelf geometry is therefore as in [3] with $D = 0$, see (1), but we now introduce a novel feature at the coast. Here we apply a Robin condition [16, 17] to model a permeable boundary (see Fig. 6).

The Robin condition is a weighted combination of Dirichlet boundary conditions and Neumann boundary conditions, and is common in many branches of physics. In our case, we can write it as

$$rv_y + v = 0, \quad y = 0, \tag{2}$$

where v is the velocity in the y direction and the subscript denotes partial derivation. Here r is a real positive quantity (the Robin parameter) that characterizes the physical conditions at the boundary. For example, if $r = 0$, we have an impermeable coastal wall. If on the other hand $r \to \infty$, then $v_y \to 0$ and there is no hindrance for particles to move through the boundary. In our case we take that r is small. Since v_y always must be finite, this means we now consider a small normal velocity at the coastline. This will be appropriate for an inner region with many narrow fjords and small islands.

In the Lofoten–Vesterålen region the relevant physical parameters typically are $H_2 = 2300\,\mathrm{m}$, $H_0 = 50\,\mathrm{m}$, $B = 60\,\mathrm{km}$ and $b = 3.2 \cdot 10^{-5}\,\mathrm{m}^{-1}$. Furthermore, the Coriolis parameter f is taken to be constant and equal to $1.3 \cdot 10^{-4}\,\mathrm{s}^{-1}$. Using mid-depth as a reference depth, the barotropic Rossby radius a_0 is typically larger than 800 km. Hence, in the shelf region $B^2/a_0^2 \ll 1$. This means that we can make the rigid lid approximation [4]. In fact, a more thorough analysis for the CSW eigen-modes, allowing for a moving surface, shows that the rigid lid approximation is indeed well fulfilled for the Lofoten region; see [6] (their Fig. 5).

Generally, the velocity components in the x, y, z directions over the shelf are u, v, w, and the surface elevation is η. Furthermore, we introduce the notation $H(y) = H_1(y)$ for simplicity. With the rigid lid approximation, the continuity equation allows for the introduction of a stream function ψ such that $\tilde{u}H = -\psi_y$, and $\tilde{v}H = \psi_x$, where a tilde denotes the linear part of the wave field. We assume that the waves are so long that the pressure is hydrostatic in the vertical direction. Neglecting any effects of friction in the shelf region, the linearized momentum equations become

$$-\psi_{ty} - f\psi_x = -gH\tilde{\eta}_x, \tag{3}$$

$$\psi_{tx} - f\psi_y = -gH\tilde{\eta}_y. \tag{4}$$

Here g is the acceleration due to gravity. We now introduce a travelling wave solution [24] by

$$\psi = H^{1/2}\varphi(y)\exp i(\kappa x - \omega t), \tag{5}$$

where κ is the complex wave number (to allow for spatial damping), and ω is the real frequency. Then the governing equations reduce to

$$\varphi'' + l^2\varphi = 0, \tag{6}$$

where the asterisk denote derivation with respect to y, and

$$l^2 = 2fb\kappa/\omega - b^2 - \kappa^2. \tag{7}$$

At the edge of the shelf $y = B$, we must generally have continuity of pressure (here surface elevation) and normal fluxes. Utilizing that the deep ocean has a flat bottom, it easy to show that the continuity conditions imply for the stream function at the shelf edge that

$$\psi_y + \kappa\psi = 0, \qquad y = B, \tag{8}$$

see [20]. In terms of the φ function in (5), the boundary condition becomes

$$\varphi' + (b + \kappa)\varphi = 0, \quad y = B. \tag{9}$$

Writing the solution to (6) as

$$\varphi = H_0^{-1/2}[A\sin l(y - B) + C\cos l(y - B)], \tag{10}$$

we find by applying (9) that $C = -lA/(b + \kappa)$. Hence,

$$\varphi = AH_0^{-1/2}[\sin l(y - B) - (l/(b + \kappa))\cos l(y - B)]. \tag{11}$$

We note right away that if the coastal boundary is impermeable, i.e. $\varphi(0) = 0$ and κ real, (11) yields the familiar relation for the eigen-modes: $\tan(lB) = -l/(b + \kappa)$, as shown in [3]. In terms of φ, we can write (2)

$$r\varphi' + (1 + rb)\varphi = 0, \quad y = 0. \tag{12}$$

Using the solution (11), we then find the complex dispersion relation from (12). It becomes

$$(b+\kappa)\sin lB + l\cos lB = -r\left[\left(b^2 + l^2 + b\kappa\right)\sin lB - l\kappa\cos lB\right]. \tag{13}$$

In this paper, we consider spatial damping, i.e.

$$\kappa = k + i\alpha, \tag{14}$$

where α/k is a small quantity. It is then seen from (7) that l is complex. We take that the modified frequency is $\omega = \omega_0 + O(\alpha/k)^2$ (to be verified later). From (7) we then obtain

$$l = l_0(1 + i\delta). \tag{15}$$

Here

$$l_0^2 = 2fbk/\omega_0 - b^2 - k^2, \tag{16}$$

while the small imaginary part is

$$\delta = (\alpha/k)[b^2 + l_0^2 - k^2]/(2l_0^2). \tag{17}$$

Inserting (16) and (17) into (7), we find

$$\omega = \omega_0(1 + \alpha^2/k^2), \tag{18}$$

as anticipated, where ω_0 is determined by (16).

Using (14), and expanding the trigonometric functions appearing in (13), we find from the real part to lowest order that

$$\tan l_0B = -l_0/(b + k), \tag{19}$$

as in [3]. From the imaginary part, we find to $O(\alpha/k)$ that

$$\alpha/k = [2Bl_0^2\{(b + k)^2 + l_0^2\}/\{\left(b^2 + l_0^2 - k^2\right)L - 2kl_0^2\}]r/B, \tag{20}$$

where $L = b + k + B(b + k)^2 + Bl_0^2$, and r/B is the small non-dimensional Robin parameter. In this problem, we can relate the attenuation coefficient directly to the group velocity $c_g = d\omega/dk$. From [20], eqn. (A.12), we find for CSWs

$$\left(b^2 + l_0^2 - k^2\right)L - 2kl_0^2 = c_g\left(b^2 + l_0^2 + k^2\right)L/c. \tag{21}$$

where $c = \omega_0/k$. By substituting into (20), we arrive at

$$\alpha/k = [2Bl_0^2\{(b + k)^2 + l_0^2\}/\{\left(b^2 + l_0^2 + k^2\right)L\}](c/c_g)(r/B). \tag{22}$$

Since c is always positive (CSWs propagate with shallow water to the right in the northern hemisphere [1]), we note from (22) that the sign of α is entirely dependent on the sign of c_g. For the present case of waves with K_1 frequency outside Lofoten, we notice from Fig. 5 that the wave number span for possible CSWs is rather small. Approximately, we find a permissible region $4 \cdot 10^{-5}\,\mathrm{m}^{-1} < k < 7 \cdot 10^{-5}\,\mathrm{m}^{-1}$, with zero group velocity for a critical wave number $k_c \approx 5.4 \cdot 10^{-5}\,\mathrm{m}^{-1}$. For $k < k_c$, the wave energy propagates northwards, and the non-dimensional damping coefficient is positive. For example, $k = 4 \cdot 10^{-5}\,\mathrm{m}^{-1}$ yields $\alpha/k = 3.0r/B$ from (22). For $k > k_c$, the group velocity is negative, and the energy propagates southwards. In this case,

with $x < 0$, we must have $\alpha < 0$ for damped waves. Taking $k = 7 \cdot 10^{-5}$ m^{-1}, we obtain $\alpha/k = -1.7r/B$ from (22).

We note that α/k in (22) becomes infinitely large when $c_g \to 0$ (positive when approached from the smaller wave number side and negative when approached from the larger wave number side). Obviously, our calculations assuming a small damping rate is not valid here, but this singular behaviour indicates that no wave energy escapes in either direction from the point where the group velocity is zero.

For the application in the nonlinear calculations in the next section, we state real parts of the linear velocity components.

$$\tilde{u} = -\psi_y/H = -[AH_0^{-1}\exp(-\alpha x - by)/(b+k)] \times [\left(bF + F'\right)\cos\theta - \delta l_0(bG + G')\sin\theta], \quad (23)$$

$$\tilde{v} = \psi_x/H = -[AH_0^{-1}\exp(-\alpha x - by)/(b+k)] \times [kF\sin\theta + (\alpha F + k\delta l_0 G)\cos\theta], \quad (24)$$

where $\theta = kx - \omega t$ is the phase function, and

$$F = (b+k)\sin l_0(y-B) - l_0\cos l_0(y-B), \quad (25)$$

$$G = (y-B)\left[(b+k)\cos l_0\,(y-B) + l_0\sin l_0(y-B)\right] - d\cos l_0(y-B). \quad (26)$$

Here

$$d = \left(b^3 + bl_0^2 - bk^2 + b^2k - l_0^2k - k^3\right)/[(b+k)(b^2+l_0^2-k^2)]. \quad (27)$$

4. The nonlinear drift problem

As demonstrated in [20], the spatial damping of the CSW field leads to nonzero radiation stresses [19] which drives the mean Lagrangian volume fluxes. In many cases of ocean wave problems, the damping is taken to be the result of bottom friction. For very long wave periods the theory by Charney and Eliassen [25] of vertical pumping in a quasi-steady Ekman bottom layer yields wave damping in the inviscid part of the fluid; see [24] for CSWs. For shorter periods (typically diurnal), the Ekman boundary layer is not properly developed, which makes this modelling dubious [26]. To avoid these problems, the usual approach is to assume a bottom stress that is linear or quadratic in the mean velocity [27].

The new idea of the present paper with a permeable coastal boundary, yields damping of the CSWs without the need to implement bottom friction. Although this makes the calculation of the radiation stress components lengthier due to the more complicated cross-shelf structure of the wave field, it simplifies considerably the derivation of the Lagrangian drift current.

In the previous sections, we considered the linearized equations. In calculating the mean drift, we need the equations to second order in wave steepness. We first define the mean nonlinear fluxes

$$\overline{U} = \overline{\int_{-H}^{\eta} u\,dz}, \quad \overline{V} = \overline{\int_{-H}^{\eta} v\,dz}, \quad (28)$$

where the over-bar denotes average over the wave cycle. These are actually the mean Lagrangian fluxes, since we integrate between material surfaces [18,28]. As before, we take that the waves are long enough to make the hydrostatic approximation. Integrating the inviscid governing equations in the vertical, and utilizing the full nonlinear boundary conditions at the free surface and the sloping bottom, we obtain for the mean quantities, correct to second order in wave steepness [18]:

$$\overline{U}_t - f\overline{V} = -gH\overline{\eta}_x + R^{(x)}, \quad (29)$$

$$\overline{V}_t + f\overline{U} = -gH\overline{\eta}_y + R^{(y)}, \quad (30)$$

$$\overline{\eta}_t = -\overline{U}_x - \overline{V}_y. \quad (31)$$

Here $R^{(x)}$, $R^{(y)}$ are the local radiation stress components; see [20], defined by

$$R^{(x)} = -\frac{1}{2}g(\overline{\tilde{\eta}^2})_x - \left(H\overline{\tilde{u}^2}\right)_x - (H\overline{\tilde{v}\tilde{u}})_y, \quad (32)$$

$$R^{(y)} = -\frac{1}{2}g(\overline{\tilde{\eta}^2})_y - (H\overline{\tilde{u}\tilde{v}})_x - \left(H\overline{\tilde{v}^2}\right)_y. \quad (33)$$

It was pointed out in [20] that since here $B^2/a_0^2 \ll 1$, the surface elevation terms in (32) and (33) are negligible compared to the velocity square terms.

We realize that the system of Eqs. (29)–(31) has time dependent free solutions (when we neglect the forcing from radiation stress terms) in the form of CSWs. These solutions vanish when we average over the wave period. We are here interested in the forced stationary solution to these equations. When $\partial/\partial t = 0$, it is found from the curl of (29) and (30) that

$$2bgH\overline{\eta}_x = R_x^{(y)} - R_y^{(x)}. \quad (34)$$

We note from (32) and (33) that if the waves are not spatially damped, i.e. if the x-derivative of the mean quantities is zero, both sides of (34) vanish, and it is not possible to determine $\overline{\eta}$. In this case, Lagrangian drift velocity along the bottom contours will contain an arbitrary part in geostrophic balance with a mean cross-shore surface tilt [29]. However, for spatially damped waves we find

$$gH\overline{\eta} = (1/(4\alpha b))\,[R_y^{(x)} - R_x^{(y)}]. \quad (35)$$

Hence, from (35)

$$gH\overline{\eta}_y = -(1/(4\alpha b))[2b\left(R_y^{(x)} - R_x^{(y)}\right) - R_{yy}^{(x)} + R_{xy}^{(y)}]. \quad (36)$$

By inserting into (30), we finally obtain for the Lagrangian mean flux

$$\overline{U} = (1/f)[R^{(y)} + (R_y^{(x)} - R_x^{(y)})/(2\alpha) + (R_{xy}^{(y)} - R_{yy}^{(x)})/(4\alpha b)]. \quad (37)$$

From the definitions (32) and (33) it is seen that $R_y^{(x)}$ and $R_{yy}^{(x)}$ are proportional to the small damping rate α. Hence, the Lagrangian mean flux along the shelf is independent of the damping rate (apart from the small amplitude attenuation). Calculation of the terms in (37) by applying (23) and (24), leads to

$$\overline{U} = \left[A^2\exp(-2\alpha x)/\left(fH_0(b+k)^2\right)\right] \times [-2k^2FF' + k^2\left(FF'' + F'^2\right)/(2b) + Q'/4 - Q''/(8b)]. \quad (38)$$

Here

$$Q = 2(bF+F')^2 - [(bF+F')\{F + \left(b^2 + l_0^2 - k^2\right)G/(2l_0)\} - \left(b^2 + l_0^2 - k^2\right)(bG+G')F/(2l_0)]', \quad (39)$$

where F and G are given by (25) and (26), respectively. The corresponding along-shore Lagrangian drift velocity then becomes

$$\overline{u}_L = \overline{U}/H. \quad (40)$$

Since the constant A in the stream function (5) has dimension m^3 s^{-1}, we can introduce a dimensional scaling factor u_0 for the drift velocity as

$$u_0 = A^2b^3\exp(-2\alpha x)/(fH_0^2). \quad (41)$$

The Lagrangian mean velocity can then be written

$$\overline{u}_L = u_0[\exp(-2by)/(8b^4\,(b+k)^2)]$$

$$\times\ [-16bk^2FF' + 4k^2\left(FF'' + F'^2\right) + 2bQ' - Q'']. \tag{42}$$

In Fig. 7 we have depicted the non-dimensional Lagrangian drift current (42) for $B = 60\,\text{km}$, and $b = 3.2 \cdot 10^{-5}\,\text{m}^{-1}$, which are typical parameter values for CSWs with diurnal frequency outside Lofoten. With reference to Fig. 5, we first consider the region where the group velocity is positive (northward propagating energy) and take $k = 4 \cdot 10^{-5}\,\text{m}^{-1}$. The corresponding value of the cross-shelf wave number then becomes $l_0 = 4.3 \cdot 10^{-5}\,\text{m}^{-1}$. Secondly, we compute the Lagrangian drift current for the case when the group velocity is negative (southward propagating energy). In this case we take $k = 7 \cdot 10^{-5}\,\text{m}^{-1}$, and $l_0 = 4.5 \cdot 10^{-5}\,\text{m}^{-1}$.

We observe from the figure that the Lagrangian drift velocity is basically located over the shallow part of the shelf with a positive value at the inner 10 km, and a distinct maximum at the coast. Between 10 km and 40 km the drift is negative (southward) with a smaller maximum value. We note that in the case of negative group velocity (dashed curve) the maximum at the coast as well as the southward flow are larger.

In the present formulation, we obtain directly the Lagrangian mean flow, as pointed out in [18]. Quite often, however, the Stokes drift [30] is taken to represent the particle drift in periodic waves. This can be misleading, as we show below.

To second order in wave steepness, the Stokes drift $\overline{u}_S$ can be written (Longuet-Higgins [31]):

$$\overline{u}_S = \overline{(\int \tilde{u}dt)\tilde{u}_x} + \overline{(\int \tilde{v}dt)\tilde{u}_y}. \tag{43}$$

It is readily found from (23) and (24) that

$$\overline{u}_S = u_0(b^2 + l_0^2 + k^2)[\exp(-2by)/(4b^4\,(b+k)^2)][2bFF' + FF'' + F'^2]. \tag{44}$$

The Stokes drift is related to the mean momentum in the wave motion, and is virtually independent of the effect of a small friction. However, as pointed out in [31], for problems with decaying waves the mean wave momentum will not be lost, but reappear as Eulerian mean currents. Hence, we can write the Lagrangian mean velocity as

$$\overline{u}_L = \overline{u}_S + \overline{u}_E, \tag{45}$$

where $\overline{u}_E$ is the mean Eulerian current. Accordingly, we have for the Eulerian mean current that

$$\overline{u}_E = \overline{u}_L - \overline{u}_S. \tag{46}$$

To compare the magnitude and spatial variation of the various non-dimensional drift components, we have plotted them in Fig. 8 for $B = 60\,\text{km}$, $b = 3.2 \cdot 10^{-5}\,\text{m}^{-1}$, $l_0 = 4.3 \cdot 10^{-5}\,\text{m}^{-1}$, and $k = 4 \cdot 10^{-5}\,\text{m}^{-1}$, i.e. positive group velocity as seen from Fig. 5.

We note that the Stokes drift (blue curve) is positive over almost the entire shelf. Accordingly, by considering only the Stokes drift, this would yield a very incomplete picture of how floating particles in the sea (cod egg and larvae, oil spill) are transported by CSWs along the shelf. In particular, one would miss the larger maximum drift velocity at the coast, as well as the negative drift over the upper part of the slope, as seen from the black curve in Fig. 8.

5. Hydrographic conditions west of Norway

West of Norway we find two northward flowing currents. Here the relatively fresh and cold Norwegian Coastal Current (NCC) is trapped at the coast. It is wedge shaped, reaching down to about 100 m at the coast, with a typical width of 50 km, and near-surface velocities of the order $0.3\,\text{m s}^{-1}$ [32]. The saltier and warmer Norwegian Atlantic Current (NwAC) is located further west. Outside Lofoten the core is typically 30 km wide. It reaches down to about 600 m, and has a maximum outside the shelf break with surface velocities of the order $0.3\,\text{m s}^{-1}$ [33]. From our results, we realize that it is the NCC, with its location over the shallow part of the shelf, which mostly may affect the Lagrangian wave-induced drift due to diurnal CSWs. In our earlier example with $B = 60\,\text{km}$, $b = 3.2 \cdot 10^{-5}\,\text{m}^{-1}$, $l_0 = 4.3 \cdot 10^{-5}\,\text{m}^{-1}$, and $k = 4 \cdot 10^{-5}\,\text{m}^{-1}$, we find that the phase speed is $c = \omega/k = 1.8\,\text{m s}^{-1}$. In this case we obtain for the group velocity from [20] that $c_g = 0.4\,\text{m s}^{-1}$. For negative group velocity, with $k = 7 \cdot 10^{-5}\,\text{m}^{-1}$, and $l_0 = 4.5 \cdot 10^{-5}\,\text{m}^{-1}$, we find $c = 1\,\text{m s}^{-1}$, and $c_g = -0.26\,\text{m s}^{-1}$. We thus see that little (if any) wave energy will be located south of Lofoten in this case.

6. Discussion and concluding remarks

Numerical modelling of the tidal motion in the Lofoten–Vesterålen region [21,22] reveals a distinct amplification of the currents for the tidal diurnal K_1 component. By analogy with the generation of CSWs due to tidal flow in the Bass strait [7–9] we suggest that the strong Moskstraumen is instrumental in generating diurnal CSWs along the narrow continental shelf outside Lofoten; see also [22]. This is supported by results from the dispersion relation, showing that CSWs with diurnal frequencies are possible in a small wave number range centred around zero group velocity.

At the inner part of the shelf west of Norway, there are a multitude of small islands and narrow fjords. We here attempt to model the effect on the CSWs when the coastal boundary is permeable, through the application of a Robin condition. This is a novel approach that leads to spatial damping of the CSWs in the inviscid region over the sloping shelf. Nonlinearly, this damping makes it possible to determine the radiation stress components that force the Lagrangian depth averaged mean current along the shelf.

As an alternative to the Robin condition, it is possible to model the coastal archipelago as an idealized macroscopic porous medium governed by Darcy's law [34], and study the wave-induced exchange of fluid between the shelf and the porous inner layer. Now continuity of normal flow and pressure (here surface elevation) must be assumed at the common permeable boundary. A similar nonlinear problem of surface waves over a porous bottom layer has been studied in [15] and in [35]. With a porous inner shelf, the damping rate becomes a function of the macroscopic permeability and the eddy viscosity. However, this modelling complicates the algebra considerably. We will therefore not pursue this idea here.

The present analysis assumes a barotropic ocean, whereas the Lofoten region in reality is stratified. Huthnance [36] has considered the effect of stratification on trapped shelf waves in terms of the Burger number; see also [37]. However, idealized numerical model runs in [38] and [39] have revealed that the effect of stratification on CSWs are small along the Norwegian shelf. This indicates that the Burger number is small, as pointed out in [6].

The most interesting result of the nonlinear analysis of the present paper is that the Lagrangian mean current is independent of the value of the damping coefficient, however small, as long as it is nonzero. This is a clear parallel to the singular behaviour of the wave-drift problem in a direct Lagrangian description. In this formulation, the limit of solutions as a small viscosity $\nu \to 0$ is different from solutions obtained with $\nu = 0$; see [40]. Since the Stokes drift represents the inviscid mean wave momentum, it is the Eulerian mean current that is independent of the magnitude of the damping in this problem. This is special, since the Eulerian mean current normally increases when the effect of friction

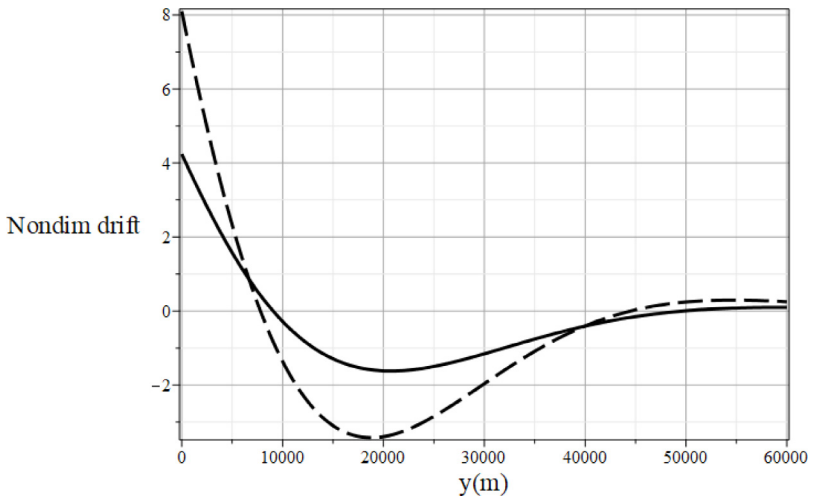

Fig. 7. The non-dimensional Lagrangian drift velocity $\overline{u}_L/u_0$ over the sloping shelf as function of the seaward coordinate. Solid curve: $k = 4 \cdot 10^{-5}\,\mathrm{m}^{-1}$ (positive group velocity). Dashed curve: $k = 7 \cdot 10^{-5}\,\mathrm{m}^{-1}$ (negative group velocity).

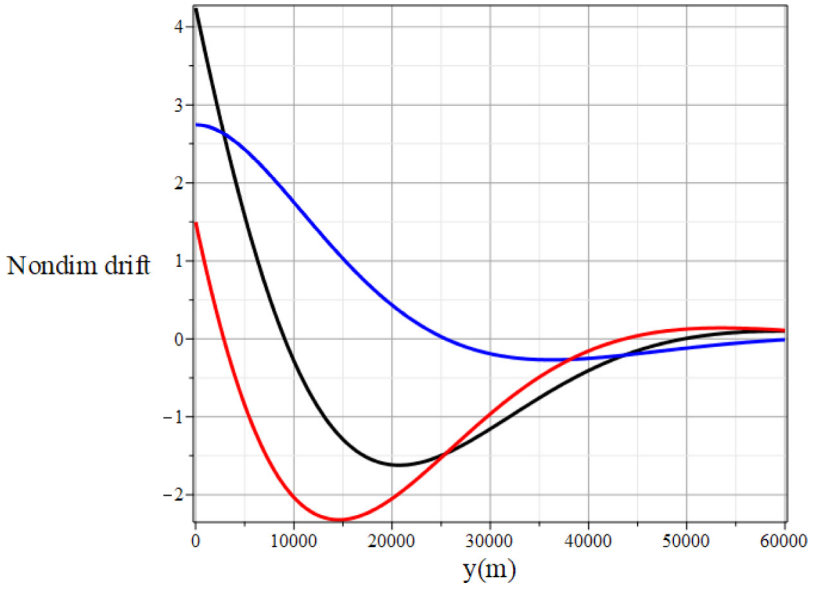

Fig. 8. Nondimensional drift velocities $\overline{u}_L/u_0$ (black), $\overline{u}_S/u_0$ (blue) and $\overline{u}_E/u_0$ (red) over the sloping shelf as function of the seaward coordinate for $k = 4 \cdot 10^{-5}\ \mathrm{m}^{-1}$ (positive group velocity). (For interpretation of the references to colour in this figure legend, the reader is referred to the web version of this article.)

(bottom friction or bulk friction) increases. In digression, it could be mentioned that for the case where the damping is caused by the interaction with an inner porous shelf instead of the Robin condition, as mentioned above, the result that the Lagrangian mean drift is independent of the damping coefficient becomes the same.

From the present calculations we note that by considering only the wave-induced Stokes drift, as often done, one would assess that particles, like cod egg and larvae, would drift northward over the entire shelf, and with a smaller speed than they actually have. This shows the importance of calculating the Lagrangian mean drift (Stokes plus Euler) when assessing wave-induced transports in the ocean. Concerning the dimensional magnitude of the Lagrangian drift, we note from Moe et al. [22] that the observed surface amplitude of the K_1 component in this area lies in the range 5–10 cm (their Table 2). If we take $\left|\tilde{\eta}_{K_1}\right| = 7$ cm as a typical value, and calculate the stream function amplitude from (3), we find that the Lagrangian drift velocity scale (41) then becomes $u_0 = 1.4\ \mathrm{cm\ s}^{-1}$. From Fig. 7 we thus infer that the dimensional Lagrangian drift velocity over the shallow part of the shelf due to the diurnal CSW is comparable in magnitude to the NCC.

Finally, it should be emphasized that the drift results for CSWs with a permeable coastal boundary is not valid only for diurnal waves as shown here, but applies in general to longer waves generated by moving weather systems over the continental shelf.

Declaration of competing interest

The authors declare that they have no known competing financial interests or personal relationships that could have appeared to influence the work reported in this paper.

Acknowledgements

The authors gratefully acknowledge support from the Research Council of Norway through Grant 280625 (JEW, travel) and by VISTA — a basic research program in collaboration between The Norwegian Academy of Science and Letters, and Equinor (EB, funding).

References

[1] M.S. Longuet-Higgins, Some dynamical aspects of ocean currents, Quart. J. R. Met.Soc. 91 (1965) 425–451.
[2] M.S. Longuet-Higgins, Double Kelvin waves with continuous depth profiles, J. Fluid Mech. 34 (1968) 49–80.
[3] V.T. Buchwald, J.K. Adams, The propagation of continental shelf waves, Proc. Roy. Soc. Lond. A 305 (1968) 235–250.
[4] A.E. Gill, E.H. Schumann, The generation of long shelf waves by the wind, J. Phys. Oceanogr. 4 (1974) 83–90.
[5] E.A. Martinsen, B. Gjevik, L.P. Røed, A numerical model for long barotropic wavesand storm surges along the western coast of Norway, J. Phys. Oceanogr. 9 (1979) 1126–1138.
[6] M. Drivdal, J.E. Weber, J.B. Debernard, Dispersion relation for continental shelfwaves when the shallow shelf part has an arbitrary width: Application to the shelf west of Norway, J. Phys. Oceanogr. 46 (2016) 537–549.
[7] V.T. Buchwald, B.J. Kachoyan, Shelf waves generated by coastal flux, Aust. J. Mar. Freshwater Res. 38 (1987) 429–437.
[8] J.F. Middleton, Long shelf waves generated by a coastal flux, J. Geophys. Res. 93 (1988) 10, 724-10, 730.
[9] R.A. Morrow, I.S.F. Jones, R.L. Smith, P.J. Stabeno, Bass strait forcing of coastaltrapped waves: ACE revisited, J. Phys. Oceanogr. 20 (1990) 1528–1538.
[10] D.E. Cartwright, Extraordinary tidal currents near St. Kilda, Nature 223 (1969) 928–932.
[11] F.-P.A. Lam, Shelf waves with diurnal tidal frequency at the greenland shelf edge, Deep-Sea Res. I 46 (1999) 895–923.
[12] A. Ommundsen, Models of cross shelf transport introduced by the Lofoten Maelstrom, Cont. Shelf Res. 22 (2002) 93–113.
[13] B. Gjevik, H. Moe, A. Ommundsen, Sources of the maelstrom, Nature 388 (1997) 837–838.
[14] R.O. Reid, K. Kajiura, On the damping of gravity waves over a permeable sea bed, Trans. Am. Geophys. Union 38 (1957) 662–666.
[15] J.J. Webber, H.E. Huppert, Stokes drift in coral reefs with depth-varying permeability, Phil. Trans. R. Soc. A 378 (2020) 20190531.
[16] K. Gustafson, Domain decomposition, operator trigonometry, Robin condition, Contemp. Math. 218 (1998) 432–437.
[17] J.E. Akin, Finite Element Analysis with Error Estimators: An Introduction To the FEMand Adaptive Error Analysis for Engineering Students, Elsevier, Butterworth-Heinemann, 2005.
[18] O.M. Phillips, The Dynamics of the Upper Ocean, Second Ed, Cambridge University Press, Cambridge, 1972.
[19] M.S. Longuet-Higgins, R.V. Stewart, Changes in the form of short gravity waves on long waves and tidal currents, J. Fluid Mech. 8 (1960) 565–583.
[20] J.E. Weber, M. Drivdal, Radiation stress and mean drift in continental shelf waves, Cont. Shelf Res. 35 (2012) 108–116.
[21] E. Børve, O.A. Nøst, P.E. Isachsen, Rectified tidal transports in Lofoten region, northern Norway, Ocean Sci. (2021) Submitted for publication.
[22] H. Moe, A. Ommundsen, B. Gjevik, A high resolution tidal model for the area around the Lofoten Islands, Cont. Shelf Res. 22 (2002) 485–504.
[23] A. Ommundsen, B. Gjevik, Scattering of tidal kelvin waves along shelves which vary intheir lengthwise direction, in: Preprint Series, Department of Mathematics, University ofOslo, 2000, p. 24.
[24] A.E. Gill, Atmosphere-Ocean Dynamics. Int. Geophys. Ser. 30, Academic Press, 1982.
[25] J.G. Charney, A. Eliassen, A numerical method for predicting the perturbations of themiddle latitude westerlies, Tellus 1 (1949) 38–54.
[26] H. Mitsudera, K. Hanawa, Effects of bottom friction on continental shelf waves, Cont. Shelf Res. 7 (1987) 699–714.
[27] E. Nøst, Calculating tidal current profiles from vertically integrated models near the critical latitude in the Barents Sea, J. Geophys. Res. 99 (1994) 7885–7901.
[28] J.E. Weber, G. Broström, Ø. Saetra, Eulerian versus Lagrangian approaches to the wave-induced transport in the upper ocean, J. Phys. Oceanogr. 36 (2006) 2106–2118.
[29] D. Moore, The mass transport velocity induced by free oscillations at a single frequency, Geophys. Fluid Dyn. 1 (1970) 237–247.
[30] G.G. Stokes, On the theory of oscillatory waves, Trans. Cam. Phil. Soc. 8 (1847) 441–455.
[31] M.S. Longuet-Higgins, Mass transport in water waves, Phil. Trans. R. Soc. A 245 (1953) 535–581.
[32] M. Mork, Experiments with theoretical models of the norwegian coastal current, in: R. Sætre, M. Mork (Eds.), The Norwegian Coastal Current, II, University of Bergen, 1981.
[33] I. Fer, A. Bosse, J. Dugstad, Norwegian atlantic slope current along the lofoten escarpment, Ocean Sci. 16 (2020) 685–701.
[34] J. Bear, Dynamics of Fluids in Porous Media, American Elsevier Publ. Comp. NY, 1972.
[35] J.E. Weber, P. Ghaffari, Wave-induced drift in a porous seabed, Env. Fluid Mech. (2021) Submitted for publication.
[36] J.M. Huthnance, On trapped waves over a continental shelf, J. Fluid Mech. 69 (1975) 689–704.
[37] L.A. Mysak, Recent advances in shelf wave dynamics, Rev. Geophys. Space Phys. 18 (1980) 211–241.
[38] B. Gjevik, Simulations of shelf sea response due to travelling storms, Cont. Shelf Res. 11 (1991) 139–166.
[39] L.H. Slørdal, E.A. Martinsen, A.F. Blumberg, Modelling the response of an idealizedcoastal ocean to a travelling storm and to flow over bottom topography, J. Phys. Oceanogr. 24 (1994) 1689–1705.
[40] J.E. Weber, Lagrangian studies of wave-induced flows in a viscous ocean, Deep-Sea Res. II 160 (2019) 68–81.